(Received 26 February 2025, Accepted 10 April 2025, Scheduled 15 April 2025)

An Ultra-Wideband All-Metal 45° Slant-Polarized 3D Vivaldi Antenna Array

Xuebo Xu[1], Shunfeng Cao[2], Qiulin Huang[1, 2, *], Lina Yang[2], and Guidong Li[2]

[1] National Key Laboratory of Radar Detection and Sensing, Xidian University, Xi'an 710071, China
[2] National Key Laboratory of Air-based Information Perception and Fusion, Luoyang 471099, China

ABSTRACT: Conventionally designed Vivaldi antennas are predominantly fabricated using PCB technology, which limits their long-term applicability in high-power systems. This paper proposes a three-dimensional all-metal slant 45°-polarized Vivaldi antenna suitable for high-power applications. The design incorporates a resonant cavity and optimized slot-line parameters to broaden the operational bandwidth. A 16×16 array configuration was developed, with parasitic elements integrated to suppress edge effects. The optimal prototype was fabricated and experimentally validated. Simulation and measurement results demonstrate that the proposed all-metal Vivaldi antenna achieves a voltage standing wave ratio (VSWR) below 2.5 across a frequency bandwidth of 6–18 GHz, along with a maximum beam scanning angle of 48°. This paper demonstrates a practical solution for balancing wideband performance (6–18 GHz) with high-power handling capabilities in phased array applications.

1. INTRODUCTION

With the rapid development of wireless communication technologies, Ultra-Wideband (UWB) technology has become a research hot spot in wireless communications, radar, and imaging systems [1–5] due to its advantages of high bandwidth, low power consumption, and high data transmission rates. As a critical component in UWB systems, antenna performance directly determines the overall system performance. Vivaldi antenna, a type of tapered slot antenna, is particularly suitable for UWB applications owing to its wide bandwidth, high gain, and excellent directivity [6]. Furthermore, antenna polarization plays a vital role in signal reception capability and anti-interference performance in complex electromagnetic environments. The slant 45° polarization, a specialized linear polarization configuration, can simultaneously receive both horizontal and vertical polarization components, demonstrating superior performance in multipolarized environments.

In recent years, extensive research on Vivaldi antennas has been conducted by scholars worldwide, proposing various structural optimizations and array design schemes. However, conventional Vivaldi antennas typically employ printed configurations [7, 8], which are fabricated using dielectric substrates and exhibit limited durability in high-power systems. These designs are generally unsuitable for high-power applications. In [9], an improved approach was proposed by integrating elliptical parasitic elements into the exponential slot line of a Vivaldi antenna, which enhanced antenna gain without compromising low-frequency performance. In [10], a novel miniaturized UWB high gain Vivaldi antenna was designed, capable of operating in the frequency range of 3.2 to 16.8 GHz. The antenna achieved a significant improvement in gain within its operating frequency range, with the maximum gain increasing from 7.6 dBi in traditional Vivaldi antennas to 10.4 dBi.

Additionally, Vivaldi arrays can be fabricated as monolithic metal components, significantly simplifying the assembly of antenna arrays. A particularly notable element design proposed in [11] and [12] achieves exceptionally wide bandwidth and performs well within the specified $\pm 45°$ scanning range. However, the elongated geometry of the antenna element leads to severe polarization degradation at the upper end of the designated frequency range when scanning exceeds 40° in the diagonal plane.

To overcome the power and durability limitations of printed Vivaldi antennas in [7, 8], we developed an all-metal Vivaldi array. Parasitic elements were added to suppress edge effects, while resonant cavities and optimized slot-lines maintained performance in a low-profile design, addressing the frequency-specific issues seen in [11, 12].

This paper aims to propose a slant 45°-polarized Vivaldi array antenna design. By optimizing the antenna structure and array layout, the proposed design seeks to enhance bandwidth, gain, and polarization characteristics.

2. ANTENNA STRUCTURE DESIGN

The all-metal Vivaldi slant-polarized antenna element is fabricated from a single sheet of metal with a thickness of $t = 3$ mm. The antenna elements are arranged in an interleaved configuration, as illustrated in Figure 1, with specific parameters detailed in Table 1. The antenna element primarily consists of three components: feeding section, transmission section, and radiation section. The feeding section employs a coaxial line to feed the antenna at its base, where a coaxial probe is inserted from

* Corresponding author: Qiulin Huang (qiulhuang@mail.xidian.du.cn).

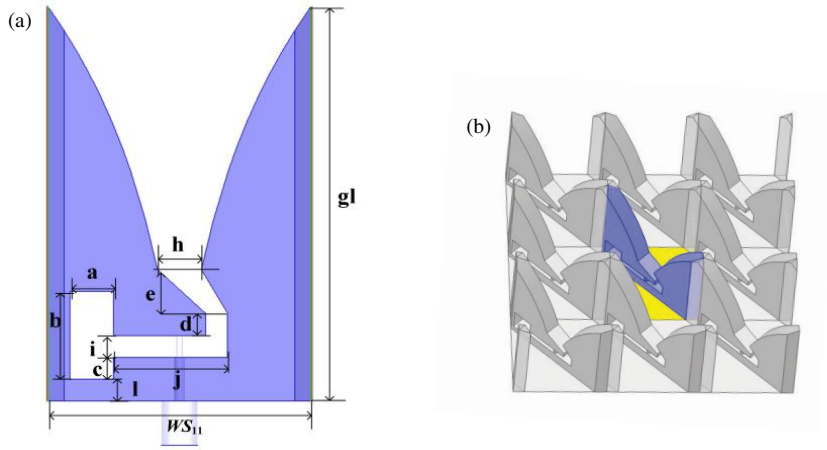

FIGURE 1. Antenna element model diagram: (a) Front view of antenna element. (b) Antenna element in array.

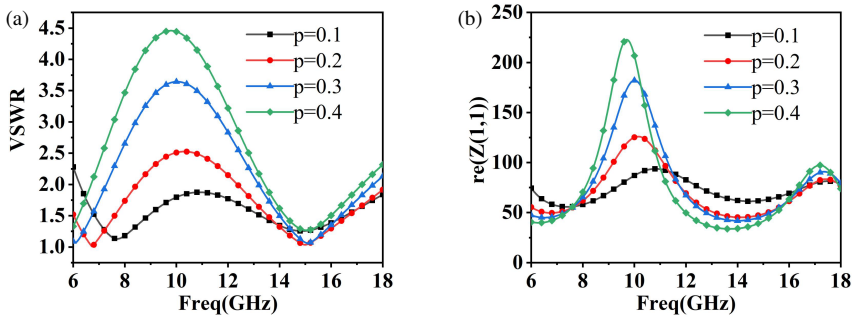

FIGURE 2. Effect of p on VSWR and antenna impedance: (a) VSWR. (b) Re(Z).

TABLE 1. Detailed parameter table of antenna element.

WS_{11}	gl	a	b	c	d
12	18	2	4	1	1
e	h	i	l	j	
2	2	1	1	5.2	

the bottom and connected to the upper metal arm of the slot line. The transmission section is composed of multiple curved slot lines, which are connected to a resonant cavity at their ends.

Based on the fundamental structure and radiation principles of the Vivaldi antenna, it is understood that for a Vivaldi antenna, the energy obtained from the inner conductor of the coaxial line is primarily radiated into free space through the exponentially tapered metal slot, enabling effective radiation of the antenna. The factors influencing the exponentially tapered slot line generally include three aspects: the width of the slot opening, the depth of the slot line, and the curvature of the slot line. The curve of the exponentially tapered slot line in a Vivaldi antenna can be expressed as [13]:

$$y = \pm (C_1 e^{px} + C_2) \tag{1}$$

where constants C_1 and C_2 are determined by the coordinates of the starting point (x_1, y_1) and the ending point (x_2, y_2) of the curve.

C_1 and C_2 can be expressed by Equation (2), as follows:

$$\begin{aligned} C_1 &= \frac{y_2 - y_1}{e^{px_2} - e^{px_1}} \\ C_2 &= \frac{y_1 e^{px_2} - y_2 e^{px_1}}{e^{px_2} - e^{px_1}} \end{aligned} \tag{2}$$

Generally, the depth of an exponentially tapered slot line is approximately one-quarter of the wavelength corresponding to the low-frequency band to ensure optimal radiation performance at lower frequencies. Therefore, for an operational frequency range of 6–18 GHz, the depth of the exponentially tapered slot line can be set to 12 mm. Figure 2 illustrates the influence of the curvature parameter p of the exponentially tapered slot line on the voltage standing wave ratio (VSWR) and impedance characteristics of the antenna. It is evident that variations in the curvature of the slot line significantly affect the impedance characteristics of the antenna in the low-frequency range, thereby impacting the antenna's transmission performance.

As the curvature p increases, the real part of the antenna's impedance in the low-frequency range gradually increases. When p exceeds 0.3, the real part of the impedance significantly surpasses 150 Ω, which is the primary reason for the notable degradation of the VSWR at the low-frequency end. When p is set to 0.1, the VSWR curve of the antenna remains predominantly below 2, indicating stable performance.

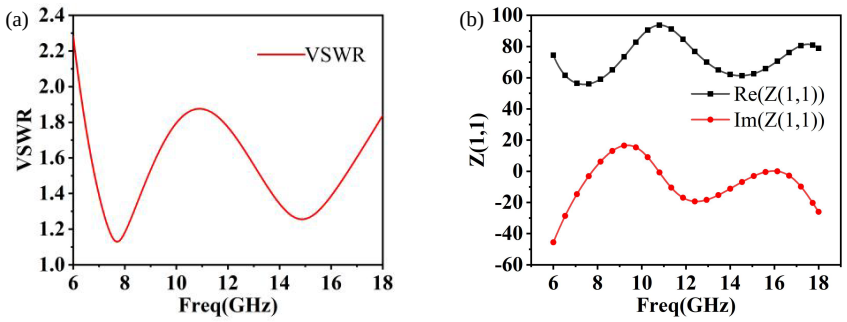

FIGURE 3. Antenna element simulation results diagram: (a) VSWR result. (b) Re(Z) and Im(Z).

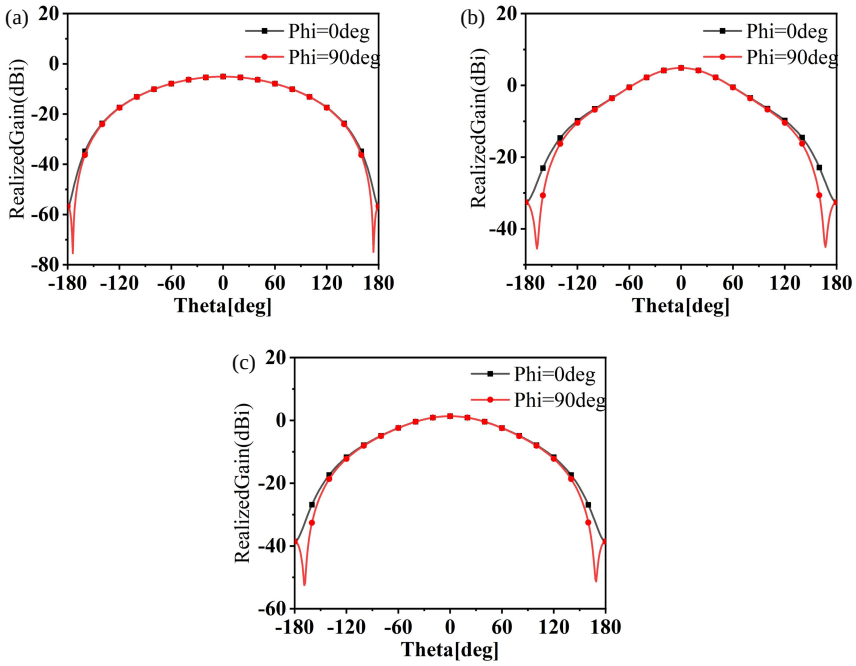

FIGURE 4. Antenna element radiation patterns. (a) 6 GHz. (b) 12 GHz. (c) 18 GHz.

These slot lines can be equivalently treated as $\lambda/4$ impedance transformers. Typically, the characteristic impedance of the slot lines differs from that of the 50-ohm coaxial line. Therefore, multiple sections of impedance transformers are necessary to achieve impedance transformation, enabling the characteristic impedance of the 50-ohm coaxial line to transition smoothly to that of the exponentially tapered slot line. This ensures excellent matching performance between the two. Moreover, at low frequencies, the resonant cavity exhibits inductive resistance, which aids in the impedance matching of the antenna. By optimizing the parameters of the resonant cavity and slot lines, as well as the antenna structure, and arranging the antenna elements in a 45-degree interleaved configuration, the antenna unit was simulated using periodic boundary conditions. The following results were obtained.

As shown in Figures 3 and 4, the performance metrics of the all-metal Vivaldi antenna element can be observed. Within the operating frequency range of 6–18 GHz, the voltage standing wave ratio (VSWR) remains below 2. The real part of the impedance oscillates slightly within the range of 55 to 90 ohms, while the imaginary part fluctuates modestly between -45 and 15 ohms. The antenna element achieves a gain of up to 4.86 dBi at 18 GHz, demonstrating excellent radiation performance.

The upper and lower ends of the slot line can be considered as a parallel-plate waveguide. The impedance of the waveguide is determined by the distance between the upper and lower plates and the width of the parallel plates. Therefore, by adjusting the width i between the slot lines, the impedance of the slot line structure also changes accordingly. Figure 5 illustrates the impact of the slot line spacing on the VSWR and input impedance. As shown in Figure 5, as the spacing i between the ends of the slot line increases, the real part of the input impedance at high frequencies also increases. This results in a mismatch between the characteristic impedance at the input port and the input impedance of the slot line, leading to a progressive deterioration of the VSWR.

As shown in Figures 6 and 7, variations in the dimensions of the rectangular resonant cavity have a significant impact on the input impedance. As the size of the rectangular resonant cavity increases, the imaginary part of the antenna's impedance grad-

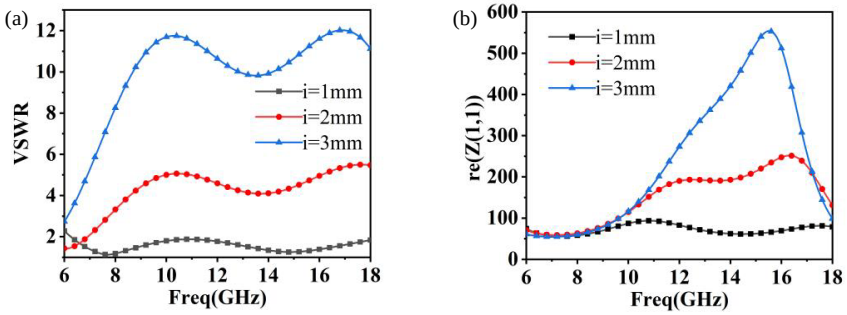

FIGURE 5. Effect of i on VSWR and antenna impedance: (a) VSWR. (b) Re(Z).

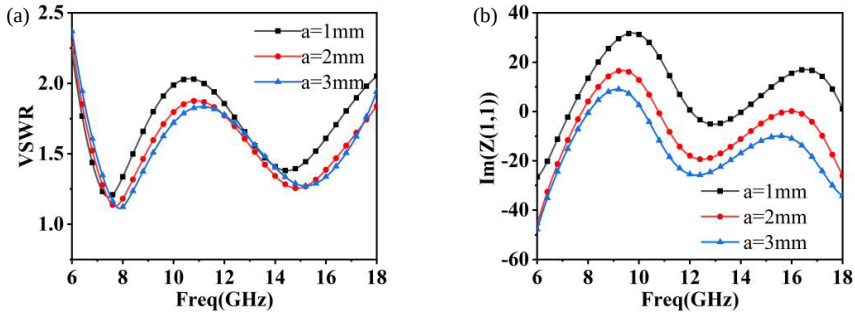

FIGURE 6. Effect of a on VSWR and antenna impedance: (a) VSWR. (b) Im(Z).

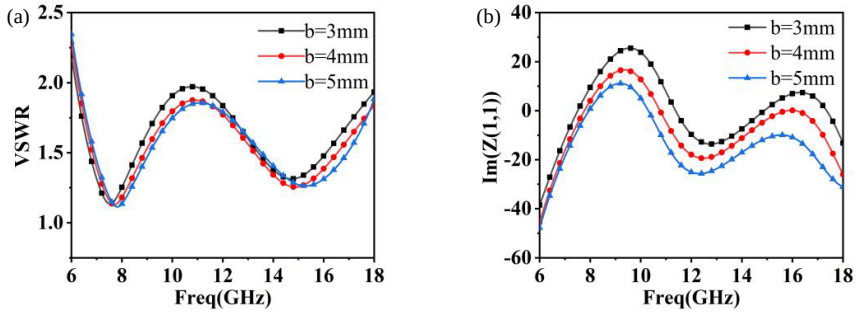

FIGURE 7. Effect of b on VSWR and antenna impedance: (a) VSWR. (b) Im(Z).

ually shifts from an inductive to a capacitive state within the 6–18 GHz frequency band, thereby affecting the antenna's radiation efficiency. When the width a of the rectangular resonant cavity is set to 2 mm and the length b to 4 mm, the imaginary part of the antenna's input impedance approaches zero. Under these conditions, most of the energy received from the feed is reflected by the rectangular resonant cavity and then transmitted through the flared metal slot to radiate into free space.

3. ANALYSIS AND DISCUSSION OF ANTENNA ARRAY RESULTS

As illustrated in Figure 8, the central region of the structure corresponds to the antenna radiating elements, while the three outermost concentric rings represent parasitic elements. Based on the antenna unit design, a 16×16 antenna array was developed. To ensure consistent performance across all array elements, three concentric rings of parasitic elements were incorporated. These parasitic elements mitigate edge effects by maintaining coupling interactions between parasitic units and edge radiating elements, thereby compensating for the absence of periodic boundary conditions at array boundaries that could otherwise degrade edge-element performance. The physical prototype of the antenna unit is shown in the accompanying figure. The entire structure was fabricated from metal and subjected to a silver-plated surface treatment to enhance operational efficiency.

As shown in Figure 9, the measurement results of the antenna array are presented. To validate the performance of the phased array configuration, a 1 : 16 power divider was integrated, enabling simultaneous activation of a column comprising 16 antenna elements. The results demonstrate that the antenna array achieves a VSWR below 2.5 across the operational frequency bandwidth. Additionally, the isolation between adjacent antenna elements exceeds 15 dB, indicating satisfactory performance of the antenna elements.

In this study, the S-parameters of the antenna array were measured by employing a 1 : 16 power divider operating across

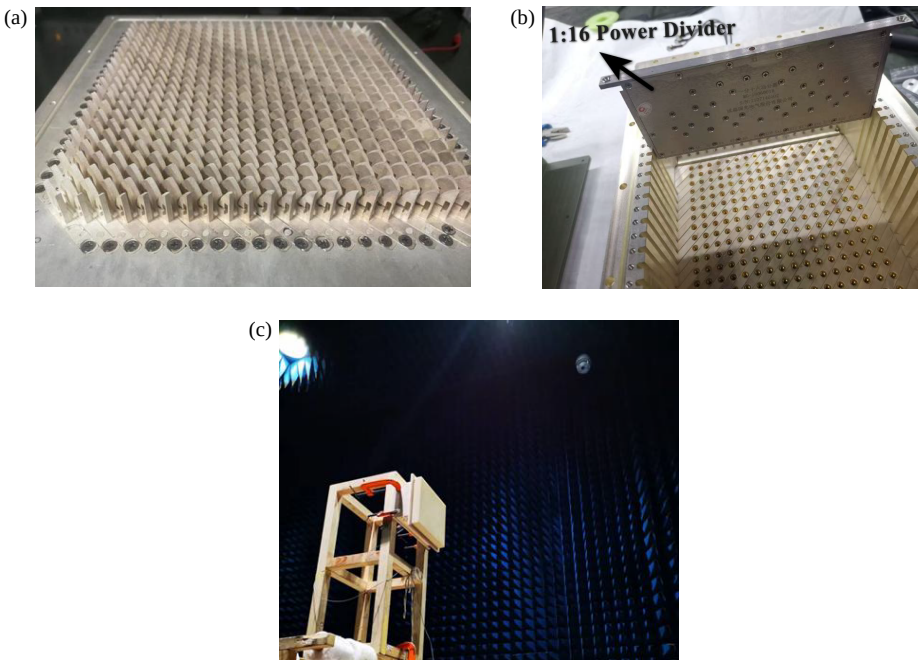

FIGURE 8. Antenna fabricated prototype. (a) Front view of the antenna array. (b) Bottom view of the antenna (integrated with 1 : 16 power divider). (c) Antenna array radiation pattern measurement setup.

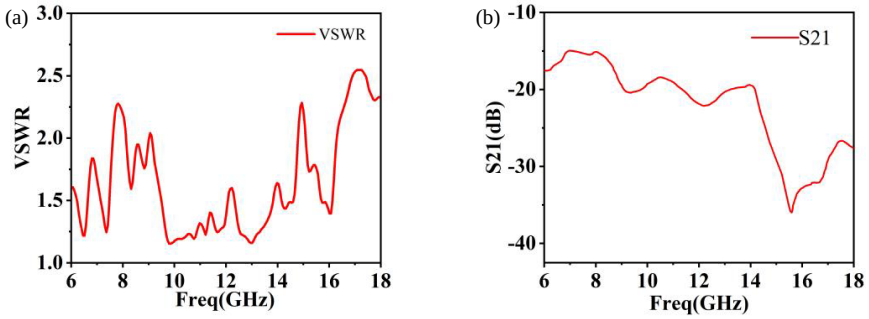

FIGURE 9. Antenna array VSWR and adjacent element isolation measurement results (including a 1 : 16 power divider). (a) VSWR. (b) S_{12}.

6–18 GHz to simultaneously feed a row of antenna elements. The measured VSWR of the array exhibited slight discrepancies compared to simulated unit-cell results. Through detailed data analysis, these differences were attributed to the introduction of the broadband power divider, which affected the impedance matching characteristics.

The measured maximum gain of individual antenna elements reached 4.86 dBi, while the 16×16 array demonstrated a peak gain of 26.19 dBi. This represents a 2.75 dB reduction from the theoretical array gain calculation of 28.9 dBi. The performance degradation primarily stems from insertion losses introduced by the power divider network within the antenna system.

As can be seen from Figure 10, the 16×16 array antenna achieves a gain of 26.19 dBi for normal beam scanning at 18 GHz, with a 3 dB beamwidth of 7°. When the beam scanning angle reaches 48°, the array gain attains 21.3 dBi. At 12 GHz, the array antenna achieves a gain of 20.77 dBi for normal beam scanning, with a 3 dB beamwidth of 9°. At a beam scanning angle of 48°, the array gain reaches 17.99 dBi. At 6 GHz, the array antenna achieves a gain of 14.24 dBi for normal beam scanning, with a 3 dB beamwidth of 19°. When the beam scanning angle reaches 48°, the array gain attains 11.05 dBi. This implementation demonstrates a practical solution for balancing wideband performance (6–18 GHz) with high-power handling capabilities in phased array applications.

Table 2 provides a detailed comparison between our all-metal Vivaldi antenna array and existing designs. The results clearly show our antenna offers several advantages. First, it achieves wider bandwidth while maintaining a lower profile. Second, it delivers excellent gain and scanning performance. The key to this performance lies in two innovative features. We have incorporated resonant cavities into the design. These cavities help maintain performance despite the reduced size. Additionally, we have added carefully optimized parasitic elements. Together, these features ensure that the antenna's gain and scanning capabilities are not compromised. Measurement data confirms our design's superiority. It outperforms conventional antennas across multiple performance metrics. The combination

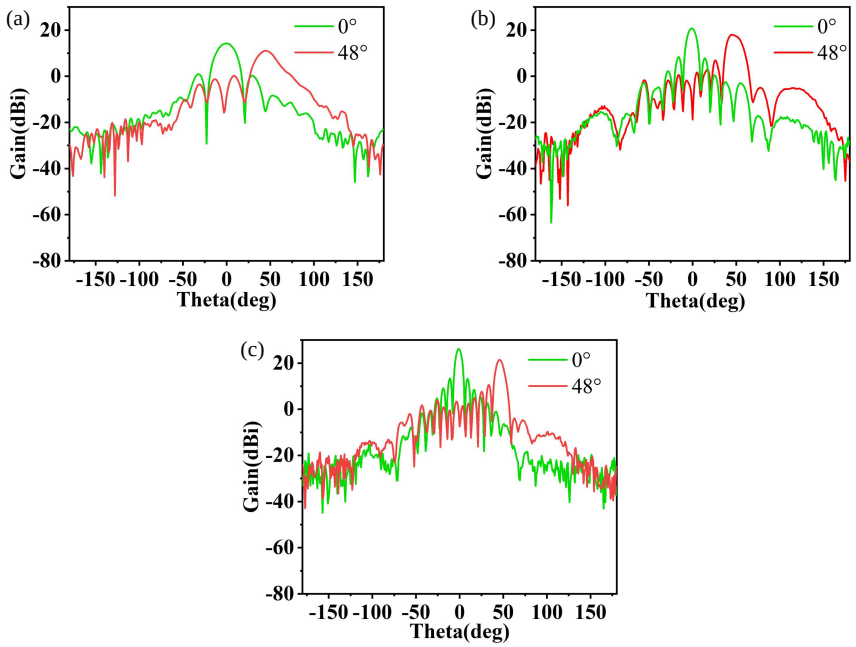

FIGURE 10. Scanning performance of the array antenna at different frequencies. (a) 6 GHz. (b) 12 GHz. (c) 18 GHz.

TABLE 2. Comparison between proposed and reported all-metal Vivaldi antenna arrays.

Ref.	Array Size (Volume (λ^3_{Max}))	Frequency (GHz) (%BW)	Scan Range	Max. Gain (dBi)	Element Spacing (λ_{Min})
[14]	8×8 $(1.42 \times 2.52 \times 0.8)$	2–6 (100%)	±45	20.0	0.59
[15]	8×8 $(2.63 \times 2.63 \times 0.87)$	26–40 (42.4%)	±60	22.0	0.51
[16]	8×8 $(1.2 \times 1.2 \times 0.75)$	10–35 (111%)	±45	20.6	0.526
This work	16×16 $(2.72 \times 2.72 \times 0.36)^{ł}$ $(3.73 \times 3.73 \times 0.36)^{łł}$	6–18 (100%)	±48	26.19	0.51

ł Effective Radiating Array of the Antenna łł Full Antenna Array with Parasitic Elements

of wide bandwidth, compact size, and stable radiation characteristics makes this array particularly valuable for practical applications. These applications include advanced radar systems and next-generation communication networks.

4. CONCLUSION

This paper proposes a three-dimensional (3D) slant 45-degree polarized Vivaldi antenna fabricated entirely from metal. The antenna element, with dimensions of $0.17\lambda\_\max \times 0.17\lambda\_\max \times 0.36\lambda\_\max$ (where $\lambda\_\max$ represents the wavelength at the lowest operating frequency), offers advantages such as low cost, low profile, and ultra-wideband performance. Furthermore, a 16×16 Vivaldi antenna array incorporating parasitic elements has been designed. The array achieves a voltage standing wave ratio (VSWR) of less than 2.5 across the operational bandwidth of 6 GHz to 18 GHz.

ACKNOWLEDGEMENT

The authors would like to thank the editors and anonymous reviewers for their efforts in evaluating our manuscript.

This project is supported by the Aeronautical Science Foundation of China, Grant No. 20220001081002.

REFERENCES

[1] Tang, M.-C., S. Xiao, T. Deng, D. Wang, J. Guan, B. Wang, and G.-D. Ge, "Compact UWB antenna with multiple band-notches for WiMAX and WLAN," *IEEE Transactions on Antennas and Propagation*, Vol. 59, No. 4, 1372–1376, Apr. 2011.

[2] Lee, D., G. Shaker, and W. Melek, "A broadband wrapped bowtie antenna for UWB pulsed radar applications," *IEEE Transactions on Antennas and Propagation*, Vol. 68, No. 12, 7803–7812, Dec. 2020.

[3] Natarajan, R., J. V. George, M. Kanagasabai, and A. K. Shrivastav, "A compact antipodal Vivaldi antenna for UWB applications," *IEEE Antennas and Wireless Propagation Letters*, Vol. 14, 1557–1560, 2015.

[4] Biswas, B., R. Ghatak, and D. R. Poddar, "A fern fractal leaf inspired wideband antipodal Vivaldi antenna for microwave imaging system," *IEEE Transactions on Antennas and Propagation*, Vol. 65, No. 11, 6126–6129, Nov. 2017.

[5] Huda, S., A. Saha, and A. Karmakar, "Ultra wideband (UWB) dielectric resonator antenna using fractal-inspired feeding mechanism," *International Journal of Communication Systems*, Vol. 36, No. 13, e5519, 2023.

[6] Liu, H., Y. Liu, W. Zhang, and S. Gao, "An ultra-wideband horizontally polarized omnidirectional circular connected Vivaldi antenna array," *IEEE Transactions on Antennas and Propagation*, Vol. 65, No. 8, 4351–4356, Aug. 2017.

[7] Liu, Y., W. Zhou, S. Yang, W. Li, P. Li, and S. Yang, "A novel miniaturized Vivaldi antenna using tapered slot edge with resonant cavity structure for ultrawideband applications," *IEEE Antennas and Wireless Propagation Letters*, Vol. 15, 1881–1884, 2016.

[8] Fei, P., Y.-C. Jiao, W. Hu, and F.-S. Zhang, "A miniaturized antipodal Vivaldi antenna with improved radiation characteristics," *IEEE Antennas and Wireless Propagation Letters*, Vol. 10, 127–130, 2011.

[9] Nassar, I. T. and T. M. Weller, "A novel method for improving antipodal Vivaldi antenna performance," *IEEE Transactions on Antennas and Propagation*, Vol. 63, No. 7, 3321–3324, Jul. 2015.

[10] Zhang, H. and F. Zhang, "A novel ultra-wideband miniature Vivaldi antenna with sawtooth outer edges and inclined elliptical slots," *IEEE Antennas and Wireless Propagation Letters*, Vol. 23, No. 9, 2708–2712, Sep. 2024.

[11] Kindt, R. W. and J. T. Logan, "Benchmarking ultrawideband phased antenna arrays: Striving for clearer and more informative reporting practices," *IEEE Antennas and Propagation Magazine*, Vol. 60, No. 3, 34–47, Jun. 2018.

[12] Kindt, R. W. and W. R. Pickles, "Ultrawideband all-metal flared-notch array radiator," *IEEE Transactions on Antennas and Propagation*, Vol. 58, No. 11, 3568–3575, Nov. 2010.

[13] Kähkönen, H., J. Ala-Laurinaho, and V. Viikari, "Dual-polarized Ka-band Vivaldi antenna array," *IEEE Transactions on Antennas and Propagation*, Vol. 68, No. 4, 2675–2683, Apr. 2020.

[14] Ohm, S., E. Kang, T. H. Lim, and H. Choo, "Design of a dual-polarization all-metal Vivaldi array antenna using a metal 3D printing method for high-power jamming systems," *IEEE Access*, Vol. 11, 35 175–35 181, 2023.

[15] Kähkönen, H., S. Proper, J. Ala-Laurinaho, and V. Viikari, "Comparison of additively manufactured and machined antenna array performance at Ka-band," *IEEE Antennas and Wireless Propagation Letters*, Vol. 21, No. 1, 9–13, Jan. 2022.

[16] Elmansouri, M. A., G. R. Friedrichs, L. B. Boskovic, and D. S. Filipovic, "An X-band through Ka-band thinned all-metal Vivaldi phased array," *IEEE Transactions on Antennas and Propagation*, Vol. 69, No. 11, 7613–7623, Nov. 2021.